Calculation of conduction-to-conduction and valence-to-valence transitions between bound states in (In,Ga)As/GaAs quantum dots

Gustavo A. Narvaez* and Alex Zunger†
National Renewable Energy Laboratory, Golden, Colorado 80401
(Dated: February 6, 2008)

We have calculated the conduction-to-conduction and valence-to-valence absorption spectrum of bound states in (In,Ga)As/GaAs quantum dots charged with up to three electrons or holes. Several features emerge: (i) In pure (non-alloyed) InAs/GaAs dots, the $1S$-$1P_1$ and $1S$-$1P_2$ conduction intraband transitions are fully in-plane polarized along $[1\bar{1}0]$ and [110], respectively, while valence transitions are weakly polarized because the hole P states do not show any in-plane preferential orientation. (ii) In *alloyed* $In_{0.6}Ga_{0.4}As$/GaAs dots the [110] and $[1\bar{1}0]$ polarization of the corresponding $1S$-$1P$ conduction intraband transitions is weakened since the two $1P$ states are mixed by alloy fluctuations. The polarization of valence intraband transitions is insensitive to changes in alloy fluctuations. (iii) For light polarized along [001], we find a strong valence-to-valence transition that involves a weakly confined hole state with predominant light-hole character. (iv) When charging the dots with a few electrons, the conduction intraband transitions display spectroscopic shifts of $\sim$ 1-2 meV. These shifts are a result of correlation effects (captured by configuration-interaction) and not well described within the Hartree-Fock approximation. (v) When charging the dots with holes, valence intraband spectra are more complex than the conduction intraband spectra as hole states are strongly affected by spin-orbit coupling, and configuration mixing is more pronounced. Spectroscopic shifts can no longer be identified unambiguously. These predictions could be tested in *single-dot* spectroscopy of n-doped and p-doped quantum dots.

I. BRIEF BACKGROUND AND SCOPE

Doping quantum dots n-type (p-type) followed by infrared-light excitation leads to conduction-to-conduction (valence-to-valence) intraband excitations between confined states. In early experiments, intraband transitions were studied for *quantum wells*,[1] where in the case of n-type doping the selection rules lead to allowed transitions only for light polarized normal to the well,[2,3,4] whereas p-type samples afforded transitions allowed in normal incidence. Instead, n-doped *quantum dots* offered the possibility of allowed intraband transitions for light incident normal to the plane of the dots. Thus, quantum dots became the focus of much experimental work devoted to study the intraband optical transitions.[5,6,7,8,9,10,11,12,13,14,15] For example, measurements of optical intraband transitions in (In,Ga)As/GaAs quantum dots charged with electron and holes have been recently performed by Zibik *et al.*[16], who measured conduction-to-conduction transitions, and Preisler *et al.*[17] who have measured valence-to-valence intraband absorption.

On the other hand, calculations of the intraband optical properties are often based on model[18,19,20] or $\mathbf{k}\cdot\mathbf{p}$[21] approaches and not high-level atomistic approaches. Here, we address this issue by calculating conduction-to-conduction and valence-to-valence intraband optical absorption of (In,Ga)As/GaAs dots charged with up to three electrons or holes. We do not intend to survey the effects of size, shape, and composition on the intraband transitions of the dots. We focus primarily on (i) the effects of alloy fluctuations on the polarization of the intraband transitions, and (ii) the differences between the absorption spectra of n-doped and p-doped dots as well as the spectroscopic shifts induced by charging. We use a combined approach to calculate the intraband absorption spectra in which we find the electron and hole single-particle states of the dots with an atomistic pseudopotential method and solve the many-particle states of charged dots within a configuration-interaction approach. The advantage of this approach over simplified methods is that it naturally includes (i) the correct symmetry of the dot; (ii) strain and alloying effects; (iii) multiband and multivalley coupling; and (iv) spin-orbit interaction. Our approach is purely electronic and does not include polaron (electron-phonon coupling) effects. We illustrate our findings with a prototypical lens-shaped $In_{0.6}Ga_{0.4}As$/GaAs dot with diameter $b = 252$ Å and height $h = 35$ Å. As a benchmark, for dots charged with a single carrier, we provide results for a pure non-alloyed InAs/GaAs dot with the same size. While so far intraband experiments have focused on ensemble of dots with different degrees of homogeneity, which broadens the observed transitions, we offer predictions that could be probed in single-dot spectroscopy of n- or p-doped dots. In addition, as the control of doping carriers is difficult, i.e in an ensemble of doped dots some have a single electron while other have two or none, we discuss the intraband spectra upon increasing the carriers one at a time.

II. METHOD: PSEUPOTENTIAL APPROACH AND CONFIGURATION-INTERACTION

We calculate the single-particle electron and hole energy levels of the self-assembled dot within an atomistic, pseudopotential-based method:[22] The wave func-

tion ψ_j and energy $\mathcal{E}_j$ are solutions of the atomistic single-particle Schrödinger equation

$$\Big[-\frac{1}{2}\nabla^2 + V_{SO} + \sum_{l,\alpha} v_\alpha(\mathbf{R}-\mathbf{R}_{l,\alpha})\Big]\psi_j = \mathcal{E}_j\,\psi_j \quad (1)$$

where v_α is the screened pseudopotential for atom of type α (In,Ga,As) with position $\mathbf{R}_{l,\alpha}$ within the dot or barrier, and V_{SO} is a non-local pseudopotential that accounts for the spin-orbit interaction.[23] These pseudopotentials are carefully fitted to bulk GaAs, InAs, and (In,Ga)As alloys, thus removing the local-density-approximation (LDA) errors. The basis in which we expand ψ_j to solve Eq. (1) is a linear combination of *full-zone* Bloch bands of the underlying solids.[24] Thus, this method incorporates multiband and multivalley coupling, band non-parabolicity, and spin-orbit effects, as well as the effects of the underlying strain in the dot and barrier.

To solve for the many-particle states $\{\Psi_\nu(\mathcal{N}),\, E_\nu(\mathcal{N})\}$ of the dot with $\mathcal{N}$ carriers, where $\mathcal{N} = N_e$ electrons or N_h holes, we use a configuration-interaction approach with screened direct (J) electron-electron and hole-hole Coulomb interaction and exchange (K).[25] This method has been recently applied to the calculation of electronic and optical properties of (In,Ga)As/GaAs dots such as electron and hole charging[26], radiative lifetimes of neutral and charged excitons,[28] relaxation times of electrons due to electron-hole Auger scattering,[29] and fine-structure splittings of neutral and charged excitons.[30]

At low temperatures such that only the ground state $\Psi_0(\mathcal{N})$ of the $\mathcal{N}$-carrier dot is significantly occupied, the optical absorption spectrum for light polarized along $\hat{\mathbf{e}}$ is given by

$$I(\hbar\omega;\hat{\mathbf{e}}) = \sum_{\nu'} |\langle\Psi_{\nu'}|\hat{\mathbf{e}}\cdot\mathbf{p}|\Psi_0\rangle|^2\delta(E_{\nu'} - E_0 - \hbar\omega). \quad (2)$$

In the results we present subsequently, we have phenomenologically broadened the spectra with a Gaussian of width $\sigma = 0.25$ meV. Such a broadening has also been used in other simulations of optical absorption in the literature.

For dots with *cylindrical* symmetry, in which the projection of the angular momentum along the cylindrical axis ($\hat{\mathbf{z}}$) is a good quantum number, the selection rules for intraband transitions are the following. For $\hat{\mathbf{e}} \parallel [100]$ or [010] transitions are allowed between states such that $\Delta L_z = \pm 1$, while for $\hat{\mathbf{e}} \parallel [001]$ only transitions with $\Delta L_z = 0$ are allowed.

We consider in our calculations prototypical lens-shaped $In_{0.6}Ga_{0.4}As$/GaAs dots with base diameter $b = 252$ Å and height $h = 35$ Å. As a benchmark, in the case of dots charged with a single carrier we also consider a pure non-alloyed InAs/GaAs dot of the same size.[27] Note that the detailed experimental characterization of the shape, size, and composition of the alloyed (In,Ga)As/GaAs dots probed optically is scarce.

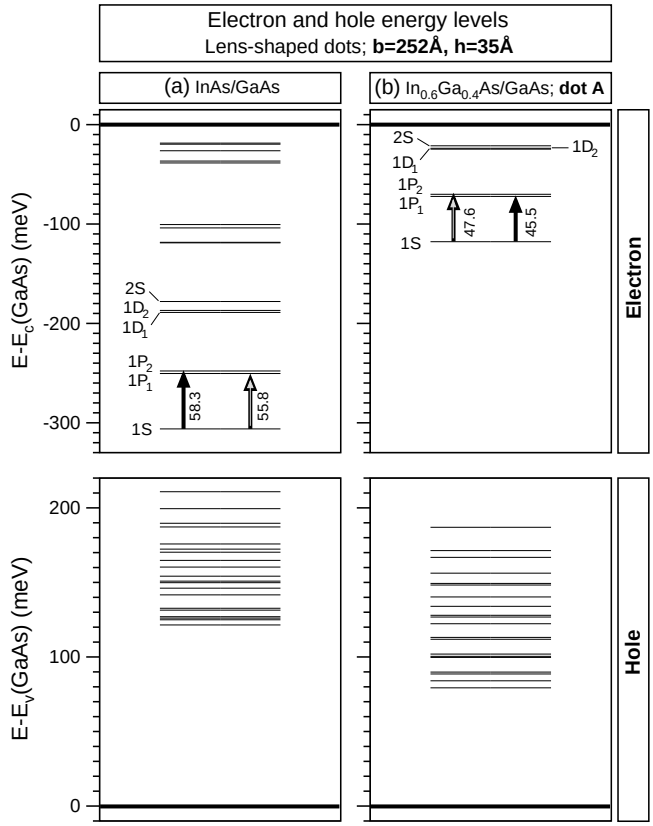

FIG. 1: Electron (top) and hole (bottom) energy levels in lens-shaped (In,Ga)As/GaAs dots with base diameter $b = 252$ Å and height $h = 35$ Å relative to the GaAs barrier conduction band minimum $E_c(\text{GaAs}) = -4.093$ eV (w.r.t vacuum) and its valence band maximum $E_v(\text{GaAs}) = -5.620$ eV (w.r.t vacuum). The energy levels are more confined in the pure (non-alloyed) InAs/GaAs dot (a) than in the alloyed $In_{0.6}Ga_{0.4}As$/GaAs dot (b). For holes, we show the first 40 confined states. Black and grey arrows indicate, respectively, the lowest intraband conduction transition for polarization along [110] and [1$\bar{1}$0]; while numbers show the transition energy in meV.

The prototypical alloyed dot we consider here presents properties like excitonic gap; electron and hole single-particle energy spacings; and binding energies of neutral and excited excitons in excellent agreement with available data.[28]

III. RESULTS FOR SINGLE-PARTICLE ELECTRON AND HOLE LEVELS

A. Electron levels

Bound states can be labeled by their leading orbital character and approximately arranged into *shells*: $\{1S;\, 1P_1, 1P_2;\, 1D_1, 1D_2, 2S;\, \ldots\}$. For the dot size considered in our calculation, a pure (non-alloyed) dot confines 15 states arranged in five shells [Fig. 1(a)], two

more shells than in its alloyed counterpart which binds 10 states [Fig. 1(b)]. The larger number of confined levels in a pure dot is due to a larger strain-modified conduction band offset than that in an alloyed dot. In the pure InAs/GaAs dot [Fig. 1(a)] the $1S$ state is located 306 meV below the conduction band minimum (CBM) of the GaAs barrier, while in the alloyed dots [Fig. 1(b)] is ~ 118 meV below the GaAs CBM. (This value changes by a few meVs depending on the random alloy fluctuations in the dot.) These energies of the $1S$ state relative to the GaAs CBM set the cutoff for conduction-to-conduction intraband transitions between bound states. The P-shell consists of two non-degenerate states $1P_1$ and $1P_2$. The origin of this splitting is atomistic[31] and a consequence of the underlying C_{2v} symmetry of the (pure, nonalloyed) dots, which is lower than $C_{\infty v}$ symmetry of the macroscopic (lens) shape, which is normally assumed in continuum effective-mass models. In our calculation we consider perfectly cylindrical dots; yet, the P-P splitting is as large as 2 meV in pure dots. Piezoelectricity[32] and non-cylindrical shape[24] further contribute to this P-P splitting. In addition, each of these P states present a nearly equal mixture of $L_z = \pm 1$ components contrary to the axially-symmetric case in which each state has a well defined L_z component. In the pure (non-alloyed) dot $1P_1$ is oriented along $[1\bar{1}0]$ and $1P_2$ is oriented along [110] [Fig. 2(a)]. In alloyed dots the symmetry of the dots is lower than C_{2v} due to random alloy fluctuations. In this case, not only [110] and $[1\bar{1}0]$ are mixed and different disorder realizations (fluctuations) change the magnitude of the P-P splitting by 1-3 meV but, more remarkably, alloy fluctuations affect the in-plane orientation (polarization) of the P states, as is shown in Fig. 2. Or, equivalently, alloy fluctuations change the relative phase $\phi_\pm$ of the $L_z = \pm 1$ components in the $1P_1$ and $1P_2$ states, which results in different in-plane orientations (polarizations) of these states. For instance, in dot A we have $\phi_+ \simeq 0$ and $\phi_- \simeq \pi/2$, while for dot C we have $\phi_+ \simeq \phi_- \simeq 0$. In turn, the D-shell consists of non-degenerate $1D_1$, $1D_2$, and $2S$ states. States $1D_1$ and $1D_2$ show a nearly even mixture of $L_z = \pm 2$ components. Depending on alloy fluctuations, state $2S$ can also have sizeable $L_z = \pm 2$ components, thus making it not possible in those cases to assign a leading orbital character to these D-shell states.

B. Hole levels

Both non-alloyed and alloyed dots confine a large ($M_h > 20$) number of single-particle levels. Due to the multi-band nature of these hole states and for flat dots like the one we consider here, only low-lying states present shell structure that is less pronounced, i.e. larger P-P and D-D splittings, than in the electron case. For these states, one can still use their leading S, P, D orbital character to identify them. Higher lying states show heavy mixing of orbital character. For pure and alloyed dots the $1S$ hole state is located, respectively, 211 meV and 186 meV above the valence band maximum of the GaAs barrier; see Fig. 1. These values are the cutoff for valence-to-valence intraband transitions between bound states. In addition, the P states are not oriented along a preferential in-plane direction [Fig. 2].

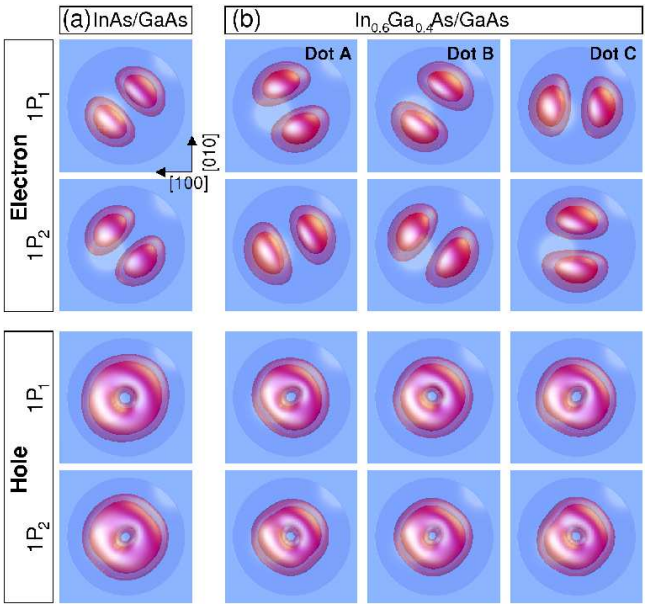

FIG. 2: (Color online) Isosurface representation of the electron (top) and hole (bottom) wavefunctions of states $1P_1$ and $1P_2$ in a pure non-alloyed InAs/GaAs dot (a), and three $In_{0.6}Ga_{0.4}As$/GaAs dots (b) with different alloy fluctuations. Dots are lens-shaped and have the same size: $b = 252$ Å and $h = 35$ Å.

IV. INTRA-CONDUCTION AND INTRA-VALENCE TRANSITIONS IN DOTS WITH A SINGLE CARRIER

Assuming that only the $1S$ state is occupied by doping, for in-plane polarized light we expect intra-conduction transitions between bound states that satisfy $\Delta L_z = \pm 1$ when the dot is occupied by a single electron. The lowest-energy transitions correspond to $1S$-$1P_1$ and $1S$-$1P_2$ (indicated by arrows in Fig. 1). The orientation (polarization) of the $1P$ states determines the polarization properties of these transitions:

(i) For pure (non-alloyed) InAs/GaAs dots, we expect that for polarization $\hat{\mathbf{e}} \parallel [1\bar{1}0]$ only transition $1S$-$1P_1$ to be allowed, while for $\hat{\mathbf{e}} \parallel [110]$ only $1S$-$1P_2$.

(ii) For alloyed dots, alloy fluctuations dictates the orientation of states $1P_1$ and $1P_2$ [Fig. 2(b)]. Thus, we expect a strong dot-to-dot dependence of the polarization properties of the two conduction intraband transitions. In particular, for the in-plane polarization $\hat{\mathbf{e}} \parallel [1\bar{1}0]$ we expect both transitions $1S$-$1P_1$ and $1S$-$1P_2$ to be allowed, with intensities

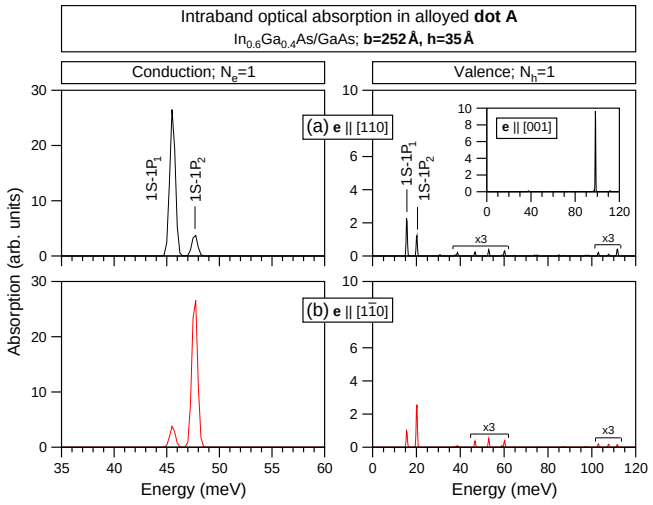

FIG. 3: (Color online) Intraband absorption spectrum for in-plane polarization $\hat{\mathbf{e}} \parallel [110]$ (a) and $\hat{\mathbf{e}} \parallel [1\bar{1}0]$ (b) in an $In_{0.6}Ga_{0.4}As/GaAs$ dot (dot A) charged with a single electron (left panels) and a single hole (right panels). For these in-plane polarizations, conduction-to-conduction transitions are nearly an order of magnitude more intense that valence-to-valence transitions (note different ordinate scales). Inset: Valence intraband transition for light polarized out-of-plane $\hat{\mathbf{e}} \parallel [001]$. The strong feature corresponds to the $1S_{hh}$-$1S_{lh}$ transition.

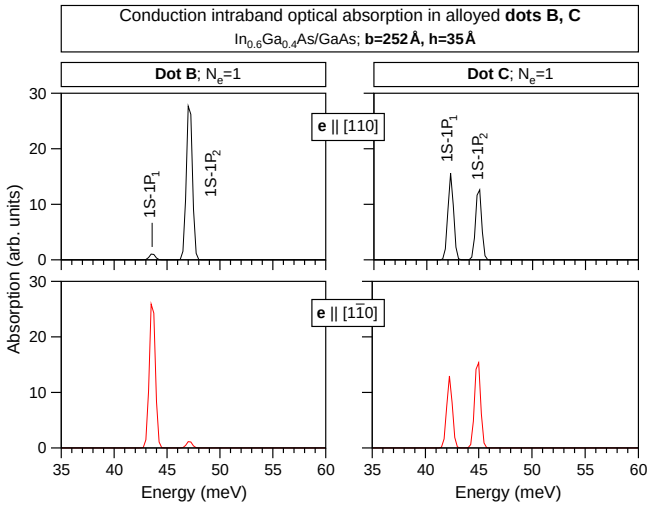

FIG. 4: *Idem* Fig. 3(a) and Fig. 3(b) for two $In_{0.6}Ga_{0.4}As/GaAs$ dots with the same size as dot A but with different random alloy fluctuations.

$$|\langle 1S|\hat{\mathbf{e}}\cdot\mathbf{p}|1P_1\rangle|^2 \propto 1-\sin(\phi_+-\phi_-) \quad (3)$$

$$|\langle 1S|\hat{\mathbf{e}}\cdot\mathbf{p}|1P_2\rangle|^2 \propto |1+\sin(\phi_+-\phi_-)|. \quad (4)$$

A. In-plane transitions

In a pure (non-alloyed) InAs/GaAs charged with one electron the lowest transition $1S$-$1P_1$ appears at 56 meV and is *fully* polarized along $[1\bar{1}0]$, while the second transition $1S$-$1P_2$ is located at 58 meV and is *fully* polarized along [110]. In contrast, in alloyed dots [Figs. 3(a) and 3(b)] we only find partial in-plane polarization: For dot A we find a transition at 46 and another at 48 meV corresponding; the lowest-energy transition $1S$-$1P_1$ is partially ($\sim 75\,\%$) polarized along $\hat{\mathbf{e}} = [110]$ while the higher-energy $1S$-$1P_2$ is partially ($\sim 75\%$) polarized along $\hat{\mathbf{e}} = [1\bar{1}0]$.

The valence intraband transitions have a smaller oscillator strength than those of the conduction transitions. For holes, as in the case of electrons, we find two strong transitions corresponding to the $1S_h$-$1P_h$ transitions. However, these transitions are weakly in-plane polarized because the hole P states do not show any preferential in-plane orientation. In addition, we also find weaker transitions in the interval 40-60 meV, which arise from the mixing between the D-shell and P-shell hole states. For dot A, the lowest valence intraband transition shows a higher intensity when light is polarized along the $[1\bar{1}0]$ direction, as in the experiment of Preisler *et al.*[17]

Calculations based on simplified models are not capable of explicitly introducing alloy fluctuations. Instead, these fluctuations are naturally included within our atomistic approach. Figure 4 illustrates the effect of random alloy fluctuations on the polarization properties of the conduction intraband transitions in $In_{0.6}Ga_{0.4}As/GaAs$ dots with the same size as dot A but different random alloy fluctuations: (i) Under $[1\bar{1}0]$ polarization, dot B presents transition $1S$-$1P_1$ nearly fully polarized and transition $1S$-$1P_2$ nearly forbidden; conversely, for $\hat{\mathbf{e}} \parallel [110]$ transition $1S$-$1P_2$ is nearly fully polarized and $1S$-$1P_1$ nearly forbidden. These polarization properties are *switched* when compared to dot A. In addition, that the lowest conduction intraband transition in *dot B* is mainly polarized along $[1\bar{1}0]$ in both is in agreement with the experiment of Zibik *et al.*[16] (ii) In contrast, dot C presents both transitions allowed for polarizations [110] and $[1\bar{1}0]$, with very small in-plane polarization anisotropies. We find that transition $1S$-$1P_1$ is polarized along [100], with transition $1S$-$1P_2$ forbidden, and that for $\hat{\mathbf{e}} \parallel [010]$ transition $1S$-$1P_2$ is allowed while $1S$-$1P_1$ is forbidden.

B. Out-of-plane polarization—intra-valence transitions

The inset of Fig. 3(a) shows the valence intraband transition for $\hat{\mathbf{e}} \parallel [001]$. We find a strong feature originated from the $1S_{hh}$-$1S_{lh}$ transition, which involves a weakly confined, highly excited hole state with predominant light-hole character. This transition is nearly three times as intense as the in-plane valence transitions. This transition is consistent with the selection rule $\Delta L_z = 0$

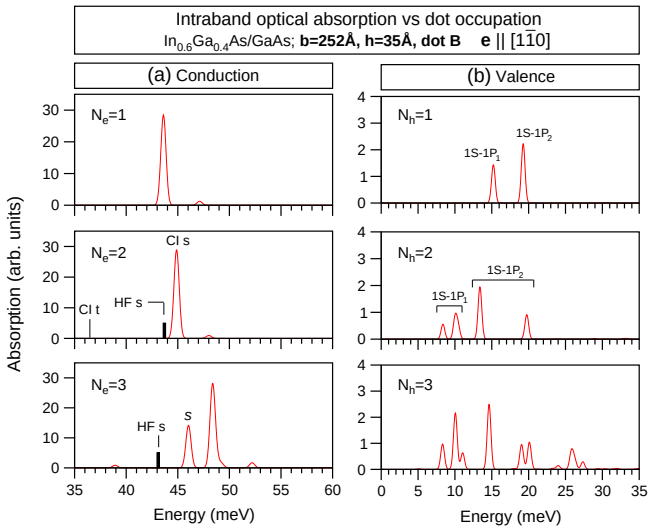

FIG. 5: (Color online) For in-plane polarization $\hat{\mathbf{e}} \parallel [1\bar{1}0]$, intraband conduction-to-conduction (a) and valence-to-valence (b) transitions calculated at the CI level versus number of electrons N_e and holes N_h in the dot. Black, short bars in panel (a) for $N_e = 2$ and 3 show the $1S$-$1P$ transition energies predicted within the Hartree-Fock approximation—Eqs. (13) and (17), respectively. For $N_e = 2$, the HF singlet (HF s) and the configuration-interaction singlet (CI s) and triplet (CI t) are indicated. The latter being forbidden.

for this light polarization.

V. INTRA-CONDUCTION AND INTRA-VALENCE TRANSITIONS IN DOTS WITH A FEW CARRIERS

We now study the conduction and valence intraband transitions for $\mathcal{N} = 2$, and 3 carriers occupying the dot.

The energy of conduction and valence band transitions in the presence of N_e electron or N_h holes is dictated by differences in total energies. [See Eq. (2).] Therefore, we expect spectroscopic shifts of the transitions upon charging. We define the intraband spectroscopic shift Δ_{if} of transition $\Psi_i \rightarrow \Psi_f$ upon adding a carrier as

$$\Delta_{if}(\mathcal{N}) = \hbar\omega_{if}(\mathcal{N}) - \hbar\omega_{if}(\mathcal{N}-1). \tag{5}$$

The energy of a many-particle state $|\Psi_\nu\rangle$ can be expressed as superposition of a Hartree-Fock term $[E^{(HF)}]$ and correlation component (δ); namely,

$$E_\nu^{(CI)}(\mathcal{N}) = E_\nu^{(HF)}(\mathcal{N}) + \delta_\nu(\mathcal{N}). \tag{6}$$

For the conduction-to-conduction intraband transition energies and shifts, we compare results for the conduction intraband transition energies and shifts obtained within the Hartree-Fock approximation and CI calculations.

A. Intra-conduction transitions vs N_e

We present Hartree-Fock (HF) expressions for the intraband transition energies when the dot is charged with $N_e = 1, 2, 3$ and then compare to configuration-interaction calculations. To illustrate our findings, we consider *dot B*, which has $1P_1$ and $1P_2$ states that are nearly fully polarized along $[1\bar{1}0]$ and $[110]$, respectively, and focus on light polarized along $[1\bar{1}0]$.

$N_e = 1$: The ground state is $|\Psi_0\rangle = |e_0^1\rangle$ and under IR light the final state is $|e_1^1\rangle$. (Both states are twofold degenerate.) For this occupation, there are no many-body effects and the energy of the initial and final state are simply given by

$$E_0(1) = \mathcal{E}_{1S}^{(e)} \tag{7}$$
$$E_f(1) = \mathcal{E}_{1P_1}^{(e)}. \tag{8}$$

The intraband transition energy is

$$\hbar\omega_{if}(1) = E_f - E_i = \mathcal{E}_{1P_1}^{(e)} - \mathcal{E}_{1S}^{(e)}. \tag{9}$$

$N_e = 2$: The closed-shell (nondegenerate) state $|\Psi_0\rangle = |e_0^2\rangle$ is the ground state, and there are four possible final states originating from $|e_0^1 e_1^1\rangle$. At the single-particle level the four final states are degenerate, but within the HF approximation these states split in a triplet (t) and a singlet (s): $|e_0^1 e_1^1\rangle_t$ and $|e_0^1 e_1^1\rangle_s$. The splitting between these states is due to the electron-electron exchange interaction, between an electron in $|S\rangle$ and an electron in $|P_1\rangle$, and equals $2\,K_{SP_1}^{(ee)}$. Under IR light excitation, only the singlet is an allowed final state. Thus, we have the following energies for the initial and final state:

$$E_0(2) = 2\,\mathcal{E}_{1S}^{(e)} + J_{SS}^{(ee)} + \delta_0(2) \tag{10}$$
$$E_f(2) = \mathcal{E}_{1P_1}^{(e)} + \mathcal{E}_{1S}^{(e)} + J_{SP_1}^{(ee)} + K_{SP_1}^{(ee)} + \delta_f(2). \tag{11}$$

This results in a $1S$-$1P$ transition energy in the presence of an extra electron that can be written as

$$\hbar\omega_{if}(2) = \mathcal{E}_{1P_1}^{(e)} - \mathcal{E}_{1S}^{(e)} + J_{SP_1}^{(ee)} + K_{SP_1}^{(ee)} - J_{SS}^{(ee)} + \big[\delta_f(2) - \delta_0(2)\big]. \tag{12}$$

Here, $J_{SS}^{(ee)}$ and $J_{SP_1}^{(ee)}$ are, respectively, the direct Coulomb interaction between two electrons in $|S\rangle$, and one electron in $|S\rangle$ and another in $|P_1\rangle$. For dot B our atomistic calculation predicts $J_{SS}^{(ee)} = 20.8$ meV and $J_{SP_1}^{(ee)} = 16.6$ meV, and $K_{SP_1} = 4.3$ meV.

Our CI calculations for $N_e = 2$ are shown in Fig. 5(a). We find that the four states arising from configuration $e_0^1 e_1^1$ indeed split in a singlet and triplet and, as expected, only the intraband transition from the ground-state to the singlet is allowed—strong feature at ~ 45 meV. The Hartree-Fock predicted transition energy [first five terms

in Eq. (12)] for dot B appears as a short black bar in Fig. 5(a) and is 43.7 meV, while CI predicts 44.9 meV, so the correlation correction [terms in brackets in Eq. (12)] is 1.2 meV.

The spectroscopic shift between the transitions in $N_e = 1$ and 2 is thus given by

$$\Delta(2) \;=\; J^{(ee)}_{SP_1} - J^{(ee)}_{SS} + K^{(ee)}_{SP_1} + \big[\delta_f(2) - \delta_0(2)\big]. \quad (13)$$

The Hartree-Fock component of this shift is 0.1 meV, whereas our CI calculation reveals a blue-shift of $\Delta(2) =$ 1.3 meV; i.e., 1.2 meV from correlation effects [terms in bracket in Eq. (13)]. This shows correlation effects determine the spectroscopic shift.

$N_e = 3$*:* The ground state of the initial state is $|e^2_0 e^1_1\rangle$ (twofold degenerate) and in addition to the final states originating from the P shell: $|e^1_0 e^1_1\rangle$ and $|e^1_0 e^1_2\rangle$, one now has six states arising from transitions to the D shell: $|e^2_0 e^1_3\rangle$, $|e^2_0 e^1_4\rangle$, and $|e^2_0 e^1_5\rangle$. The energy of the ground state and the P-shell derived final are the following:

$$E_0(3) \;=\; 2\,\mathcal{E}^{(e)}_{1S} + \mathcal{E}^{(e)}_{1P_1} + J^{(ee)}_{SS} + 2\,J^{(ee)}_{SP} - K^{(ee)}_{SP} + \delta_0(3) \quad (14)$$

$$E_{fP}(3) \;=\; 2\,\mathcal{E}^{(e)}_{1P_1} + \mathcal{E}^{(e)}_{1S} + 2\,J^{(ee)}_{SP} + J^{(ee)}_{PP} + \delta_f(3). \quad (15)$$

Here, $J^{(ee)}_{PP}$ is the direct Coulomb interaction of two electrons occupying $|P_1\rangle$. For dot B, $J^{(ee)}_{PP} = 16.0$ meV. The resulting $1S$-$1P_1$ intraband transition energy is

$$\hbar\omega_{0f}(3) = \mathcal{E}^{(e)}_{1P_1} - \mathcal{E}^{(e)}_{1S} + J^{(ee)}_{P_1P_1} - J^{(ee)}_{SS} + K^{(ee)}_{SP_1} + \big[\delta_f(3) - \delta_0(3)\big]. \quad (16)$$

For dot B, the HF component amounts to 43.1 meV [black bar in Fig. 5(a)] and the term due to correlations (in brackets) amounts to 2.9 meV.

The spectroscopic shift between the $1S$-$1P_1$ transitions in $N_e = 2$ and 3 is

$$\Delta(3) = J^{(ee)}_{P_1P_1} - J^{(ee)}_{SP_1} + \big[\delta_f(3) - \delta_f(2) - \delta_0(3) + \delta_0(2)\big]. \quad (17)$$

The HF part is a red-shift of $\Delta(3) = -0.6$ meV. The value predicted by EMA is nearly twice as big; namely, $[\Delta(3)]_{EMA} = -1.3$ meV. Yet, our CI calculation shows [Fig. 5(a) for $N_e = 3$] that the transition is actually *blue-shifted* by 1.1 meV with respect to that in $N_e = 2$. The correlations contribution [in brackets in Eq. (17)] being 1.7 meV. Note also that the intensity of transition $1S$-$1P_1$ is bleached (reduced) by nearly 50 % as a consequence of Pauli blocking—one electron occupies $|1P_1\rangle$.

Regarding the P-D transitions, within the HF approximation we expect them to occur at the following energies:

$$\hbar\omega_1(3) \;=\; \mathcal{E}^{(e)}_{1D_1} - \mathcal{E}^{(e)}_{1P_1} + 2\,J^{(ee)}_{SP_1} - K^{(ee)}_{SP_1} - 2\,J^{(ee)}_{SD_1} - K^{(ee)}_{SD_1} + \delta_1(3) \quad (18)$$

$$\hbar\omega_2(3) \;=\; \mathcal{E}^{(e)}_{1D_2} - \mathcal{E}^{(e)}_{1P_1} + 2\,J^{(ee)}_{SP_1} - K^{(ee)}_{SP_1} - 2\,J^{(ee)}_{SD_2} - K^{(ee)}_{SD_2} + \delta_2(3) \quad (19)$$

$$\hbar\omega_3(3) \;=\; \mathcal{E}^{(e)}_{2S} - \mathcal{E}^{(e)}_{1P_1} + 2\,J^{(ee)}_{SP_1} - K^{(ee)}_{SP_1} - 2\,J^{(ee)}_{S2S} - K^{(ee)}_{S2S} + \delta_3(3) \quad (20)$$

We find in our CI calculations [Fig. 5(a)] that the strong feature around 49 meV corresponds to the (nearly overlapping) $1P$-$1D_1$ and $1P$-$1D_2$ transitions. The weak transition at ~ 52 meV arises from $1P_1$-$2S$ and because $|2S\rangle$ in the alloyed dot is primarily oriented (polarized) along [110] the transition is weak.

B. Valence transitions vs N_h

Earlier calculations assumed simple models with the incorrect symmetry and neglected the multiband nature of the hole single-particle states, which leads to an incorrect treatment of the hole-hole interaction. Within our atomistic approach, spin-orbit coupling and the multiband nature of the hole single-particle states prevent us from writing meaningful HF expressions in the case of *holes*. So we discuss directly the results of our CI calculations. Figure 5(b) shows the valence intraband transitions for $N_h = 1$, 2, and 3 for light polarized along $\hat{\mathbf{e}} \parallel [1\bar{1}0]$. In general, compared to the conduction case, the valence intraband spectra are more sensitive to the number of holes in the dot.

$N_h = 2$*:* The $1S$-$1P_1$ transition (lowest feature in $N_h = 1$) appears red-shifted by nearly 6 meV and split—two peaks between 8-11 meV. Due to the hole-hole exchange interaction this transition is split in a pair of low-energy, nearly doubly degenerate states and two higher-lying states mutually split by ~ 1 meV. Similarly, transition $1S$-$1P_2$ splits in two transitions: One transition at ~ 14 meV, with an ensuing red-shift of 6 meV, and another at ~ 20 meV that appears slightly blue-shifted

(~ 1 meV) with respect to the transition at $N_h = 1$.

Note that contrary to the case of electrons, and due to the presence of spin-orbit interaction, the four states arising from the two-hole configuration $h_0^1 h_2^1$ do not split in a triplet and one singlet. Instead, these four states split in two doublets that are allowed under IR light excitation. More importantly, in the commonly used EMA with two-dimensional harmonic confinement and without spin-orbit coupling one would not find these double-peak structure of allowed transitions, but instead one would find a spectra that resembles that of the $N_e = 2$ electron case.

$N_h = 3$*:* While the ground state is well described by $|h_0^2 h_1^1\rangle$, the effect of configuration mixing in the final states (upon absorption) due to hole-hole interaction is remarkably pronounced and leads to a complex spectrum. As a result, it is not possible to determine unambiguously the spectroscopic shifts $\Delta(3)$. Prominent features are the following.

(i) The lowest-energy peak at nearly 9 meV corresponds to transition $1S$-$1P_1$. Also, the peak at ~ 15 meV is mainly $1S$-$1P_1$, but mixed with $1P_1$-$2S$ and $1P_1$-$2S$. This mixing leads to the high intensity of this transition. Remarkably, we find that in contrast to the $N_e = 3$ case, the $1S$-$1P_1$ transition *is not bleached* by having a hole occupying the $1P_1$ state.

(ii) The peak at 10 meV correspond to transition $1S$-$1P_2$, while the weaker feature at ~ 11 meV is due to a transition with $1P_1$-$1D_1$ predominant character.

(iii) Above 15 meV the features in the spectrum correspond to transitions to heavily mixed final configurations: (a) The lower-energy peak in the double-peak structure around 20 meV corresponds to a mixture of the allowed $1S$-$1P_1$ and $1S$-$1P_2$ transitions in addition to a sizeable component (16%) of the forbidden $h_0^2 h_1^1$-$h_0^1 h_2^2$ transition. In turn, the higher-energy peak is a mixture of $1S$-$1P_2$ and $1P_1$-D_1 transitions. (b) The peak at 26 meV arises from two nearly overlapping transitions. These transitions are a mixture of allowed P-D and P-F transitions, as well as forbidden transitions.

(iv) Although *significantly weaker* than the other features in the spectrum, the peak at 24 meV corresponds to a forbidden transition made allowed by configuration mixing with allowed transitions. We also have found this type of transitions in the *interband* spectra of (In,Ga)As/GaAs dots.[33]

VI. SUMMARY

By combining an atomistic, pseudopotential-based approach with the configuration method, we have calculated the conduction and intraband transitions in (In,Ga)As/GaAs quantum dots with up to three carriers. We illustrated our calculations with a prototypical lens-shaped $In_{0.6}Ga_{0.4}As$/GaAs dot with diameter $b = 252$ Å and height $h = 35$ Å. And as a benchmark, for dots charged with a single carrier, we provided results for a pure non-alloyed InAs/GaAs dot with the same size. We have made specific predictions that could be probed in *single-dot* infrared spectroscopy of *n*-doped and *p*-doped dot:

(i) In pure, non-alloyed InAs/GaAs dots, the $1S$-$1P$ conduction intraband transitions are fully in-plane polarized, while valence transitions are weakly polarized because the hole P states do not show any in-plane preferential orientation.

(ii) In alloyed $In_{0.6}Ga_{0.4}As$/GaAs dots the in-plane polarization of $1S$-$1P$ conduction intraband transitions strongly depend on alloy fluctuations, which change the in-plane orientation of the nearly generate P-shell states. The polarization of valence intraband transitions is insensitive to changes in alloy fluctuations.

(iii) Upon changing the number of carriers in the dot, the intraband transitions display spectroscopic shifts of about 1-2 meV. These shifts are not well described within Hartree-Fock, instead their magnitude is determined by correlation effects.

(iv) Spin-orbit coupling and the multi-band characteristic of holes states result in important differences between the *many-particle* valence and conduction intraband spectra. Spectroscopic shifts can only be determined unambiguously for conduction transitions.

Acknowledgments

This work was funded by the U.S. Department of Energy, Office of Science, Basic Energy Sciences, under contract No. DE-AC36-99GO10337 to NREL, and by NREL Director's DDRD program.

* Current address: Eclipse Energy Systems, Inc., St. Petersburg, Florida 33710; Electronic address: gnarvaez@eclipsethinfilms.com

† Electronic address: alex˙zunger@nrel.gov

[1] For a review on nearly the first decade of work on quantum well infrared detectors see B. F. Levine, J. Appl. Phys. **74**, R1 (1993).

[2] L. C. West and S. J. Eglash, Appl. Phys. Lett. **46**, 1156 (1985).

[3] B. F. Levine, R. J. Malik, J. Walker, K. K. Choi, C. G. Bethea, D. A. Kleinman, and J. M. Vandenberg, Appl. Phys. Lett. **50**, 273 (1986).

[4] H. C. Liu, M. Buchanan, and Z. R. Wasilewski, Appl. Phys. Lett. **72**, 1682 (1998).

[5] H. Drexler, D. Leonard, W. Hansen, J. P. Kotthaus, and P. M. Petroff, Phys. Rev. Lett. **73**, 2252 (1994).

[6] M. Fricke, A. Lorke, J. P. Kotthaus, G. Medeiros-Ribeiro, and P. M. Petroff, Europhys. Lett. **36**, 197 (1996).

[7] S. Sauvage, P. Boucaud, J.-M. Gérard, and V. Thierry-Mieg, Phys. Rev. B **58**, 10562 (1998).

[8] S. Sauvage, P. Boucaud, J.-M. Gérard, and V. Thierry-Mieg, J. Appl. Phys. **84**, 4356 (1998).

[9] L. Chu, A. Zrenner, G. Böhm, and G. Abstreiter, Appl. Phys. Lett. **75**, 3599 (1999).

[10] L. Chu, A. Zrenner, G. Böhm, and G. Abstreiter, Appl. Phys. Lett. **76**, 1944 (2000).

[11] S. Sauvage, P. Boucaud, T. Brunhes, V. Immer, E. Finkman, and J.-M. Gérard, Appl. Phys. Lett. **78**, 2327 (2001).

[12] K. Goede, A. Weber, F. Guffarth, C. M. A. Kapteyn, F. Heinrichsdorff, R. Heitz, D. Bimberg, and M. Grundmann, Phys. Rev. B **64**, 245317 (2001).

[13] S. Hameau, J. N. Isaia, Y. Guldner, E. Deleporte, O. Verzelen, R. Ferreira, G. Bastard, J. Zeman, and J. M. Gérard, Phys. Rev. B **65**, 085316 (2002); S. Hameau, Y. Guldner, O. Verzelen, R. Ferreira, G. Bastard, J. Zeman, A. Lemaître, and J. M. Gérard, Phys. Rev. Lett. **83**, 4152 (1999).

[14] B. Aslan, H. C. Liu, M. Korkusinski, S.-J. Cheng, and P. Hawrylak, Appl. Phys. Lett. **82**, 630 (2003).

[15] E. A. Zibik, A. M. Adawi, L. R. Wilson, A. Lemaître, J. W. Cockburn, M. Hopkinson, and G. Hill, J. Appl. Phys. **100**, 013106 (2006).

[16] E. A. Zibik, A. D. Andreev, L. R. Wilson, M. J. Steer, R. P. Green, W. H. Ng, J. W. Cockburn, M. S. Skolnick, and M. Hopkinson, Physica E **26**, 105 (2005).

[17] V. Preisler, R. Ferreira, S. Hameau, L. A. de Vaulchier, and Y. Guldner, M. L. Sadowski, and A. Lemaître, Phys. Rev. B **72**, 115309 (2005).

[18] A. Wojs and P. Hawrylak, Phys. Rev. B **53**, 10841 (1996).

[19] J.-P. Leburton, L. R. C. Fonseca, J. Shumway, D. Ceperley, and R. M. Martin, Jpn. J. Appl. Phys. **38**, 357 (1999).

[20] J.-Z. Zhang and I. Galbraith, Appl. Phys. Lett. **84**, 1934 (2004).

[21] H. Jiang and J. Singh, Appl. Phys. Lett. **71**, 3239 (1997).

[22] A. Zunger, phys. stat. sol. (b) **224** , 727 (2001).

[23] A. J. Williamson, L.-W. Wang, and A. Zunger, Phys. Rev. B **62**, 12963 (2000).

[24] L.-W. Wang and A. Zunger, Phys. Rev. B **59**, 15806 (1999).

[25] A. Franceschetti, H. Fu, L. W. Wang, and A. Zunger, Phys. Rev. B **60**, 1819 (1999).

[26] L. He and A. Zunger, Phys. Rev. B **73**, 115324 (2006); L. He, G. Bester, A. Zunger, Phys. Rev. Lett. **95**, 246804 (2005).

[27] In reality one expects the dots to be alloyed due to interdiffusion, making pure InAs/GaAs dots an idealization. However, Schmidt *et al.* [Phys. Rev. B **54**, 11346 (1996)] and others have presented data that show exciton recombination at about 1 eV, which has been attributed to pure non-alloyed InAs/GaAs dots.

[28] G. A. Narvaez, G. Bester, and A. Zunger, Phys. Rev. B **72**, 245318 (2005).

[29] G. A. Narvaez, G. Bester, and A. Zunger, Phys. Rev. B **74**, 075403 (2006).

[30] G. Bester, S. Nair, and A. Zunger, Phys. Rev. B **67**, 161306 (2003); M. Ediger, G. Bester, B. D. Gerardot, A. Badolato, P. M. Petroff, K. Karrai, A. Zunger, and R. J. Warburton (unpublished).

[31] G. Bester and A. Zunger, Phys. Rev. B **71**, 045318 (2005).

[32] G. Bester, A. Zunger, X. Wu, and D. Vanderbilt, Phys. Rev. B **74**, 081305(R) (2006).

[33] G. A. Narvaez and A. Zunger, Phys. Rev. B **74**, 045316 (2006).